



HAL
open science

Synthesis and Characterization of Metallic (Fe-Ni, Fe-Ni-Si) Reference Materials for SIMS $^{34}\text{S}/^{32}\text{S}$ Measurements

Célia Dalou, Lenny Riguet, Johan Villeneuve, Laurent Tissandier, Thomas Rigaudier, Damien Cividini, Julien Zollinger, Guillaume Paris

► **To cite this version:**

Célia Dalou, Lenny Riguet, Johan Villeneuve, Laurent Tissandier, Thomas Rigaudier, et al.. Synthesis and Characterization of Metallic (Fe-Ni, Fe-Ni-Si) Reference Materials for SIMS $^{34}\text{S}/^{32}\text{S}$ Measurements. *Geostandards and Geoanalytical Research*, In press, pp.1-14. 10.1111/ggr.12584. hal-04680729

HAL Id: hal-04680729



<https://hal.science/hal-04680729v1>

Submitted on 29 Aug 2024

HAL is a multi-disciplinary open access archive for the deposit and dissemination of scientific research documents, whether they are published or not. The documents may come from teaching and research institutions in France or abroad, or from public or private research centers.

L'archive ouverte pluridisciplinaire **HAL**, est destinée au dépôt et à la diffusion de documents scientifiques de niveau recherche, publiés ou non, émanant des établissements d'enseignement et de recherche français ou étrangers, des laboratoires publics ou privés.

Synthesis and Characterization of Metallic (Fe-Ni, Fe-Ni-Si) Reference Materials for SIMS $^{34}\text{S}/^{32}\text{S}$ Measurements

Celia Dalou (1)* , Lenny Riguet (1, 2), Johan Villeneuve (1), Laurent Tissandier (1), Thomas Rigaudier (1), Damien Cividini (1), Julien Zollinger (3) and Guillaume Paris (1) 

(1) Université de Lorraine, CNRS, CRPG, F-54000 Nancy, France

(2) Laboratoire Magmas et Volcans, Université Clermont Auvergne, CNRS UMR 6524, OPGC-IRD, F-63000 Clermont-Ferrand, France

(3) Institut Jean Lamour, Department of Metallurgy and Materials Science and Engineering, Campus ARTEM, Allée André Guinier, Université de Lorraine, Nancy F-54011, France

* Corresponding author. e-mail: celia.dalou@univ-lorraine.fr

Secondary ion mass spectrometry (SIMS) is often used to determine the sulfur contents and isotope ratios of metallic alloys in meteorites or high-pressure experimental samples. However, SIMS analyses involve calibration and the determination of instrumental mass fractionation in reference materials with a matrix composition similar to that of the unknown samples. To provide metallic reference materials adapted to S measurements via SIMS, we synthesised a series of twenty-eight alloys comprising four FeNi(\pm Si) compositions ($\text{Fe}_{95}\text{Ni}_5$, $\text{Fe}_{90}\text{Ni}_{10}$, $\text{Fe}_{80}\text{Ni}_{20}$, and $\text{Fe}_{80}\text{Ni}_{15}\text{Si}_5$) with S contents varying from $100 \mu\text{g g}^{-1}$ to $4 \text{ g}/100\text{g}$ using the “melt spinning” method, which guarantees that the metal alloys are rapidly quenched at $\sim 10^6 \text{ K s}^{-1}$. Sulfur contents were determined at the Service d'Analyse des Roches et Minéraux at the CRPG and absolute $\delta^{34}\text{S}$ values were determined by multi-collector ICP-MS (MC-ICP-MS, ThermoScientific Neptune) and isotope ratio mass spectrometry (ThermoScientific Delta V). A $\delta^{34}\text{S}$ value of $16.01 \pm 0.31\text{‰}$ was consistently obtained using the MC-ICP-MS, which was indistinguishable of the $\delta^{34}\text{S}$ value of the FeS starting material ($15.95 \pm 0.08\text{‰}$). It suggests that S did not undergo isotopic fractionation during the melting process. Of fifteen samples containing $\leq 5000 \mu\text{g g}^{-1}$ S, SIMS measurements with $15\text{-}\mu\text{m}$ -diameter spots were repeatable to within 10% relative (1 standard deviation, 1s) for S contents and 2‰ for $\delta^{34}\text{S}$ values. However, samples containing $> 5000 \mu\text{g g}^{-1}$ S showed FeNi-FeS immiscibility, leading to minor dispersion of the S mass fractions and $\delta^{34}\text{S}$ values. No matrix effect was observed for Fe-Ni, Si, or S contents in terms of the calibration curves and instrumental mass fractionation. We ultimately recommend eight samples as reliable reference materials for S isotopic measurements by SIMS, which we can share worldwide with other laboratories.

Keywords: sulfur, metal, SIMS, reference materials, isotope ratios, MC-ICP-MS.

Received 06 Mar 24 – Accepted 05 Aug 24

The stable (non-radiogenic) S isotopic compositions of planetary reservoirs are key cosmochemical tracers used to determine the origin(s) of S on Earth. However, discrepancies between the S isotopic compositions of Earth's rocks ($\delta^{34}\text{S} = -1.4 \pm 0.5\text{‰}$; Labidi *et al.* 2013) compared with those of chondrites ($-0.3 \pm 0.2\text{‰}$ in enstatite chondrites and $-0.08 \pm 0.44\text{‰}$ to $+0.49 \pm 0.16\text{‰}$ in carbonaceous chondrites; Wang *et al.* 2021) imply that a process fractionated the terrestrial $\delta^{34}\text{S}$ values from those of Earth's precursors. Among planetary processes that could have fractionated the $\delta^{34}\text{S}$ values of Earth's mantle, core formation is a likely candidate, given the siderophile (‘iron-loving’) character of S (Tsunoi *et al.* 2018, Li *et al.* 2016).

High-pressure experimental samples are used to quantify elemental and isotopic fractionations during core formation (e.g., Labidi *et al.* 2016). Bulk measurements are commonly performed to accurately determine isotopic fractionations of between 0.15 and 0.30‰ at the 2s level (Labidi and Cartigny 2016, Labidi *et al.* 2016). This method, described in Labidi *et al.* (2012, 2016), requires that metal and silicate phases be hand separated under a binocular microscope to obtain 20–50 mg of silicate and 2–10 mg of metal alloy. Although these amounts are representative of what can be obtained in experimental samples, the typical S abundances in the alloys of Labidi *et al.* (2016) were between ~ 9 and $\sim 23\%$ *m/m*, making them iron-

doi: 10.1111/ggr.12584

© 2024 The Author(s). *Geostandards and Geoanalytical Research* published by John Wiley & Sons Ltd on behalf of International Association of Geoanalysts.

This is an open access article under the terms of the [Creative Commons Attribution-NonCommercial-NoDerivs](https://creativecommons.org/licenses/by-nc-nd/4.0/) License, which permits use and distribution in any medium, provided the original work is properly cited, the use is non-commercial and no modifications or adaptations are made.

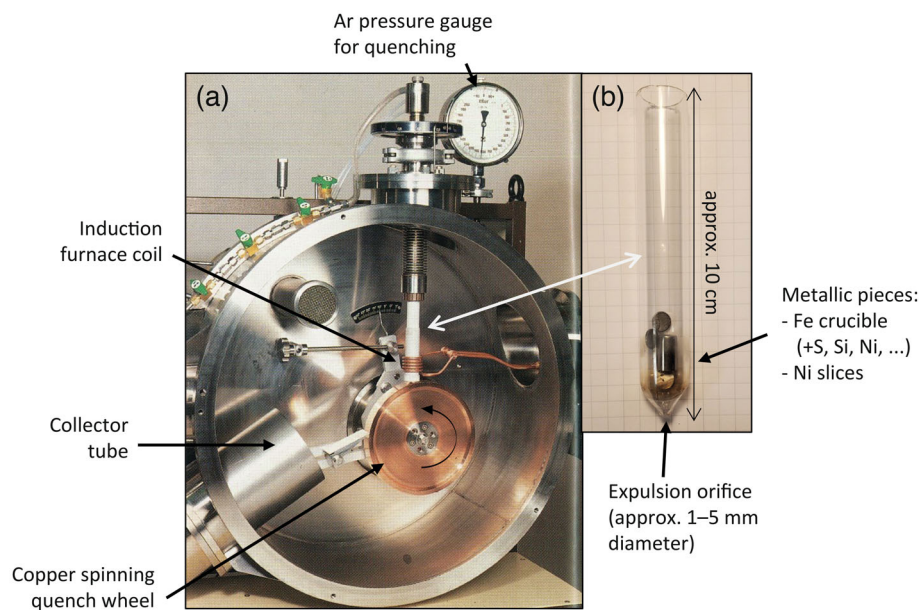


Figure 1. The melt-spinning device used to synthesise alloys in this study. (a) View of the interior (~70 cm in diameter). A door closes the device volume (~100 l) to establish an inert gas atmosphere (here, Ar) during synthesis. (b) The silica sample tube (15 mm external diameter) containing the filled Fe crucible (containing FeS powder \pm Si lumps) and Ni slices (as well as additional Si pieces, as needed) to be melted.

sulfides. When only trace amounts of S are present, i.e., concentrations of hundreds to thousands of parts per million, several hundred milligrams are required for reproducible S extraction and S isotopic analyses by isotope ratio mass spectrometry (IRMS). Such sample amounts cannot be obtained in high-pressure experiments.

In multiphase experimental samples containing metal blobs smaller than 30 μm in diameter (Dalou *et al.* 2017, Speilmanns *et al.* 2019) and distributed randomly throughout the silicate phase, bulk chemical analyses cannot be performed. Therefore, local microanalyses of S contents and isotopic ratios must be performed by secondary ion mass spectrometry (SIMS). SIMS measurements allow for local analyses of areas as small as 10 μm in diameter, and thus small volumes corresponding to a few nanograms, in a matter of minutes. However, SIMS measurements require appropriate reference materials to overcome matrix effects, which partly depend on phase chemistry and structure. However, no available S-bearing metallic reference materials have been adapted to SIMS measurements, which require homogeneous alloys, i.e., molten metals quenched very rapidly, and with matrices similar to those of the metal blobs obtained in high-pressure experimental samples.

Here, we present a novel set of metallic SIMS reference materials, synthesised using the “melt-spinning” method, which

guarantees the very efficient quenching of metal alloys of different compositions (Tkatch *et al.* 2002). The absolute S mass fractions of these alloys were determined using a carbon-sulfur analyser and their isotopic compositions were cross-calibrated by IRMS and multi-collector ICP-MS (MC-ICP-MS); their homogeneities of Fe-Ni and Si mass fractions were verified by SEM and EPMA, whereas their homogeneities in S mass fractions and $\delta^{34}\text{S}$ values were verified by SIMS.

Metal alloy synthesis

We prepared Fe-Ni alloys in proportions of 95 mass % Fe and 5 mass % Ni (sample prefix ‘F95-’), 90 mass % Fe and 10 mass % Ni (‘F90-’), 80 mass % Fe and 20 mass % Ni (‘F80-’), and 80 mass % Fe, 15 mass % Ni, and 5 mass % Si (‘FeSi-’). Two to three grams of starting materials were prepared by coring Fe rods to prepare Fe crucibles and filling them with FeS powder \pm Si lumps. Then, the Fe crucibles were welded shut using Fe discs (slices of the same Fe rods) and loaded into a quartz sample tube (Figure 1). Finally, the Fe/Ni ratios and Si contents were adjusted by adding Ni slices and additional Si lumps (as needed) alongside the filled Fe crucible in the quartz sample tube. For each Fe-Ni composition, FeS powder was added to achieve nominal S contents of 100 $\mu\text{g g}^{-1}$ (sample suffix ‘-S1’), 400 $\mu\text{g g}^{-1}$ (‘-S4’), 1000 $\mu\text{g g}^{-1}$ (‘-S10’), 5000 $\mu\text{g g}^{-1}$ (‘-S50’), 1

Table 1.
Major element compositions (in g/100 g) determined by EPMA, carbon-sulfur analyser and, for selected samples, IRMS

Samples	Fe	Ni	Si	S (EPMA)	S (CS analyser)	S (IRMS)	n	S (recalculated from SIMS)*
F95S1	94.70 ± 0.37	4.88 ± 0.04		bdl	0.02 ± 0.01		9	0.018 ± 0.002
F95S4	94.84 ± 0.37	4.92 ± 0.08		0.10 ± 0.16	0.07 ± 0.01		6	0.060 ± 0.006
F95S10	94.93 ± 0.41	4.97 ± 0.08		0.10 ± 0.07	0.11 ± 0.01		6	0.14 ± 0.01
F95S50	94.36 ± 0.41	4.95 ± 0.05		0.52 ± 0.07	0.51 ± 0.07		12	0.54 ± 0.04
F95SP1	92.01 ± 0.28	6.68 ± 0.08		1.04 ± 0.12	1.00 ± 0.02		6	1.12 ± 0.03
F95SP2	92.71 ± 0.36	5.04 ± 0.05		2.19 ± 0.10	1.88 ± 0.02		6	1.81 ± 0.19
F95SP4	86.81 ± 0.42	3.53 ± 0.09		6.16 ± 0.07	5.52 ± 1.02		12	5.11 ± 0.35
F90S1	89.38 ± 0.38	10.50 ± 0.26		bdl	0.02 ± 0.02		9	0.015 ± 0.004
F90S4	89.64 ± 0.66	9.95 ± 0.08		0.04 ± 0.03	0.07 ± 0.06		18	0.057 ± 0.004
F90S10	89.71 ± 0.63	10.06 ± 0.29		0.17 ± 0.30	0.12 ± 0.01		12	0.11 ± 0.02
F90S50	89.01 ± 0.27	10.29 ± 0.04		0.56 ± 0.06	0.52 ± 0.01		6	0.54 ± 0.03
F90SP1	88.07 ± 0.55	10.43 ± 0.05		1.02 ± 0.09	0.91 ± 0.16		24	1.07 ± 0.17
F90SP2	87.07 ± 0.31	10.33 ± 0.09		2.43 ± 0.25	1.62 ± 0.28		6	1.84 ± 0.10
F90SP4	82.39 ± 0.49	11.36 ± 0.08		5.71 ± 0.21	5.15 ± 0.03		14	4.67 ± 0.36
F80S1	79.38 ± 0.35	20.06 ± 0.10		bdl	0.02 ± 0.02		6	0.009 ± 0.001
F80S4	79.96 ± 0.40	19.62 ± 0.16		0.06 ± 0.03	0.06 ± 0.02		9	0.064 ± 0.003
F80S10	79.70 ± 0.40	19.95 ± 0.12		0.08 ± 0.05	0.12 ± 0.01	0.07 ± 0.02	6	0.12 ± 0.02
F80S50	79.54 ± 0.22	19.75 ± 0.09		0.54 ± 0.05	0.50 ± 0.01	0.35 ± 0.07	6	0.52 ± 0.05
F80SP1	78.72 ± 0.50	19.94 ± 0.17		1.15 ± 0.37	1.02 ± 0.01	0.84 ± 0.14	6	1.15 ± 0.03
F80SP2	72.57 ± 0.25	24.05 ± 0.13		3.14 ± 0.22	2.54 ± 0.01			
F80SP4	73.39 ± 0.27	20.92 ± 0.12		5.33 ± 0.19	4.69 ± 0.06	4.35 ± 0.17	6	4.78 ± 0.66
FeSiS1	80.88 ± 0.42	14.11 ± 0.07	5.43 ± 0.07	bdl	0.02 ± 0.02		15	0.011 ± 0.003
FeSiS4	80.93 ± 1.13	14.05 ± 0.60	5.48 ± 0.42	0.03 ± 0.02	0.04 ± 0.01		27	0.043 ± 0.005
FeSiS10	80.86 ± 0.42	13.96 ± 0.17	5.57 ± 0.13	0.09 ± 0.04	0.10 ± 0.03		12	0.09 ± 0.01
FeSiS50	82.77 ± 0.28	12.24 ± 0.08	4.52 ± 0.04	0.76 ± 0.04	0.68 ± 0.01		6	0.76 ± 0.05
FeSiSP1	78.39 ± 0.46	14.90 ± 0.09	5.30 ± 0.07	1.06 ± 0.02	0.95 ± 0.02		6	1.20 ± 0.13
FeSiSP2	75.66 ± 1.01	15.69 ± 0.29	5.90 ± 0.10	2.52 ± 0.80	1.95 ± 0.02			
FeSiSP4	74.85 ± 0.45	15.39 ± 0.07	4.97 ± 0.06	4.67 ± 0.12	4.41 ± 0.11		6	4.35 ± 0.33

SIMS data were recalculated using the recommended calibration (slope 0.0039 ± 0.0002 obtained from the calibration curves – section 5). Uncertainties reflect 1s standard deviations on twelve analyses per sample by EPMA, three analyses by CS analyser and IRMS, and n analysis for SIMS.

g/100 g (noted ‘-SP1’), 2 g/100 g (‘-SP2’), and 4 g/100 g (‘-SP4’). These S contents of the starting materials are only estimates based on weights measured during sample preparation on a balance with precision of 0.02 mg. We prepared a total of twenty-eight compositions (Table 1). The Fe-Ni-S (\pm Si) alloys were synthesised at the Jean Lamour Institute in Nancy (France) using the melt spinning quenching technique (Figure 1), summarised as follows. The samples were placed in a 13-mm inner diameter quartz tube that was pierced with a 1–1.2 mm orifice at its bottom (Figure 1b). Samples were melted by induction melting (at 3.5 to 4 kW) for a few seconds under flowing argon to prevent oxidation. The molten alloy was then ejected using an Ar overpressure through the tube’s circular orifice and onto the outer surface of the rapidly rotating copper quenching wheel (22 cm in diameter). The estimated quench rate using this method can vary from 10^4 to 10^6 K s⁻¹ (Tkatch *et al.* 2002).

Between each experiment, the outer surface of the wheel was polished with 1200 grit polishing paste, the chamber

vacuum was cleaned, and the entire interior was cleaned with ethanol.

Each Fe-Ni-S (\pm Si) composition required a unique induction power and melting duration, requiring that the melting procedure be adapted while under live visual observation. Therefore, incomplete melting occasionally occurred, resulting in final compositions too far from the target compositions; in those cases, we repeated the synthesis experiments.

Measurement techniques

Sample observation and characterisation

The textures of all samples were observed visually (Figure 2) and carefully studied by SEM at the CRPG in backscattered electron mode at high magnification and chemically mapped to check for the presence of exsolved

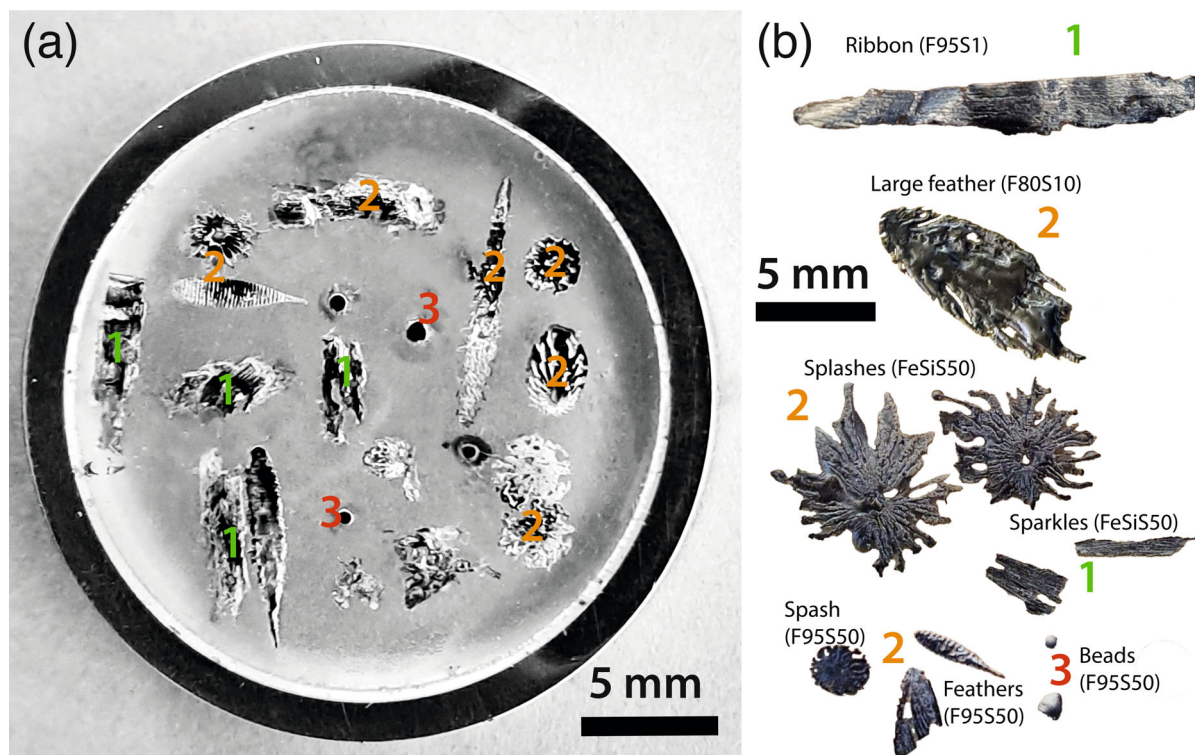


Figure 2. Different samples obtained during the melting spinning experiments: 1, ribbons and sparkles; 2, feathers and splashes; and 3, beads. (a) Resin mount prepared for SEM analysis. (b) Enlarged views of example textures with sample numbers indicated. When possible, only the type-1 textures were analysed because they were the most homogeneous and quenched the fastest.

sulfide (Figure 3), and determined the homogeneity of Fe, Ni, Si and S contents in the samples to a first approximation.

Iron, Ni, Si, and S mass fractions of the synthetic metal alloys were analysed on the JEOL JXA 8230 EPMA at the CRPG using a 15 keV accelerating voltage and 15 nA beam current. Spot analyses were performed on samples with low S concentrations (all samples with $\leq 1000 \mu\text{g g}^{-1}$ S and F95S50) because they did not show any micro-textures or heterogeneities at first glance. A defocused beam (15 μm diameter) was used for samples with $\geq 5000 \mu\text{g g}^{-1}$ S to average compositional heterogeneities, as described in the results section. Count times were 20 s on-peak and 10 s off-peak for all elements. Certified pure Fe, Ni, and Si metals (Thermo Scientific™; certified purities of 99.95%, 99.98%, and 99.9999%, respectively) were used as reference materials for their respective elements, and pyrite for S. Reference materials were analysed at the beginning and end of every session, and every four samples to monitor

any instrumental drift during the analysis of the metal alloys.

The data were processed with the PhiRhoZ method, which typically yields a bias within 2% on reference materials. Here, this procedure yielded S detection limits of 0.02 g/100 g in pyrite and in the alloys.

Carbon-sulfur analyser

The S contents of samples were determined using the HORIBA EMIA-320V2 Carbon-Sulfur (CS) analyser HORIBA EMIA-320V2 by Service d'Analyse des Roches et Minéraux (SARM) at the CRPG. Triplicates of 50 ± 2 mg of each sample were analysed. Samples were heated by induction in ceramic crucibles to > 1450 °C. Once a sample was completely molten, the released gases were oxidised by an oxygen flux, dehydrated (to avoid any interferences between H_2O and SO_2 peaks), and cleaned in a series of filters (to remove any chlorides or dust). For each analysis, the total

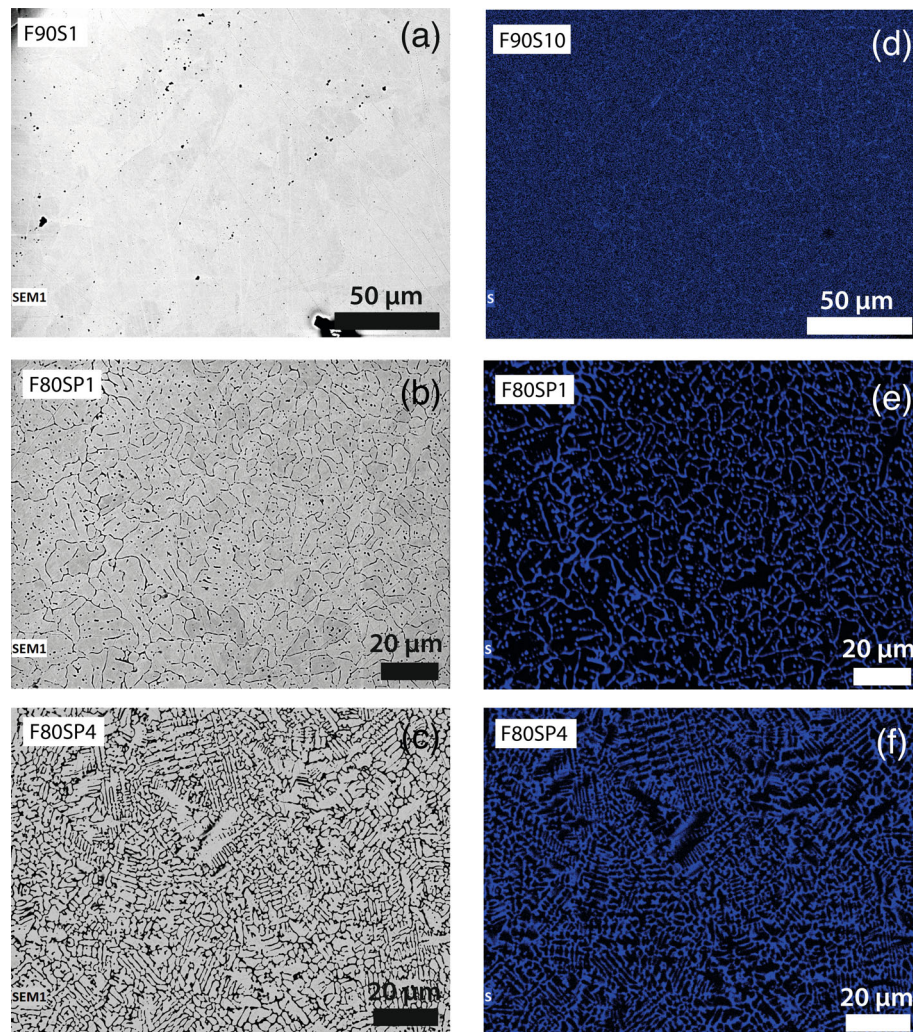


Figure 3. (a–c) Backscattered electron images showing sample textures: (a) metallic crystallisation in sample F90S1 (nominally containing $100 \mu\text{g g}^{-1}$ S), (b) immiscibility texture in F80SP1 ($1 \text{ g}/100 \text{ g S}$), and (c) quench texture in F80SP4 ($4 \text{ g}/100 \text{ g S}$). (d–f) SEM chemical maps of sulfur showing the scales of S heterogeneities in samples with different S contents: (d) $1000 \mu\text{g g}^{-1}$ (F90S10), (e) $1 \text{ g}/100 \text{ g}$ (F80SP1), and (f) $4 \text{ g}/100 \text{ g}$ (F80SP4). The same sample areas are shown in (b) and (e) and in (c) and (f).

amounts of CO , CO_2 , and SO_2 gases released were measured. Sodium metabisulfite ($\text{Na}_2\text{S}_2\text{O}_5$) reference materials (VWR Chemicals™, AnalaR NORMAPUR quality, purity 99.3%), dried at 105°C , were used as measurement standards for instrument calibration, whereas two to four certified SARM reference materials (iron ore reference materials and silicate glasses or minerals) were used for quality control purposes after every five sample analyses.

This method achieves a S determination limit of $100 \mu\text{g g}^{-1}$. This limit is based on statistics from SARM measurements, not from manufacturer of the CS analyser. The relative standard deviations on these measurements (calculated

from repeated measurements – over years – of reference materials) were $> 20\%$ for S contents $< 500 \mu\text{g g}^{-1}$, $< 20\%$ for contents of $500\text{--}1000 \mu\text{g g}^{-1}$, $< 10\%$ for contents of $1000\text{--}5000 \mu\text{g g}^{-1}$, and $< 5\%$ for contents $> 5000 \mu\text{g g}^{-1}$.

Sample preparation and S isotopic measurement by MC-ICP-MS

Sulfur isotopic ratio measurements of these metal alloys and the starting FeS powder by MC-ICP-MS required that we develop a novel dissolution procedure to extract S from the metallic matrix. Different sample masses were weighed in

PTFE beakers according to their sulfur content: ~ 10 mg sample for $< 1000 \mu\text{g g}^{-1}$ S, ~ 5 mg for $1000 \mu\text{g g}^{-1}$ to $1 \text{ g}/100 \text{ g S}$, and ~ 1 mg for $\geq 1 \text{ g}/100 \text{ g S}$. We prepared twenty-six samples, three of which (F95S10, F9OSP4, and FeSi50) were treated in triplicate to test the repeatability of the dissolution procedure, as follows. First, samples were left for ~ 24 h in 1 ml of hydrogen peroxide to be oxidised and to prevent the loss of sulfur by H_2S degassing during dissolution if the oxidation rate was slower than the dissolution rate. The hydrogen peroxide was then evaporated on a hot plate at 90°C before adding $400 \mu\text{l}$ of *aqua regia* (1/3 pure distilled HNO_3 and 2/3 pure distilled HCl) to dissolve the samples and recover the S as sulphates. All acids ($\sim 15 \text{ mol l}^{-1}$ for HNO_3 and $\sim 11.5 \text{ mol l}^{-1}$ for HCl) are distilled at the CRPG with a Savilex™ DST-1000 system. The reaction was accelerated at 80°C . The solution was evaporated at 95°C (sulfate is not volatile at temperatures below 100°C ; Freyer and Voigt 2003), ultra-pure water (resistivity: $18.2 \text{ M}\Omega \text{ cm}$) was added, and the solution was centrifuged. The solution was neutralised using $80 \mu\text{l}$ of distilled ammonia, which allowed the iron and nickel oxides to precipitate. Oxides and sulfates were then separated by centrifugation. The supernatant was collected and dried before being diluted in 1 ml of ultra-pure water.

Sample purification was performed by ion chromatography on BioRad disposable columns containing 0.8 ml of AG1X8-type resin. The resin was first rinsed twice with ten column volumes (CVs) of $\sim 1.5 \text{ mol l}^{-1}$ HNO_3 , then twice with 10 CVs of $\sim 3.8 \text{ mol l}^{-1}$ HCl.

The resin was conditioned with one rinse of 10 CVs of 0.5% HCl. The sample was then introduced, and the resin was rinsed three times with 7 CVs of ultra-pure water to ensure the removal of unwanted elements and leave only the sulfate in the column. Once only the sulfate remained in the column, the complete elution of the sulfate was recovered with three rinses of 2 CVs of 0.45 mol l^{-1} HNO_3 (Paris *et al.* 2013, Paris 2023). The final volume was then evaporated to remove the excess HNO_3 and keep only the sulfate ions as sulfuric acid.

The $^{34}\text{S}/^{32}\text{S}$ isotopic ratios were measured against Vienna Canyon Diablo Troilite (as $^{34}\text{S}/^{32}\text{S}_{\text{VCDT}}$) on the Neptune Plus MC-ICP-MS at the CRPG. The samples were introduced after dilution with a 5% v/v HNO_3 solution to reach a sulfate concentration of $17.5 \mu\text{mol l}^{-1}$, i.e., 87.5% of the Na_2SO_4 bracketing isotope standard solution (BISS, $20 \mu\text{mol l}^{-1}$). Sodium was added from a NaOH solution to the test solutions to match the Na^+ concentration of the BISS. The total volume of the samples analysed was 2 ml. Each diluted sample was analysed twice using the

standard-bracketing approach (Paris *et al.* 2013, Paris 2023). The $^{34}\text{S}/^{32}\text{S}_{\text{VCDT}}$ isotope ratios (sample or bracketing standard) were obtained by measuring fifty cycles of 4.194 s of the intensities of ^{32}S and ^{34}S simultaneously. The instrumental background was measured after each sample or standard analysis and was subtracted from the mean signal. Aberrant and/or problematic sections of the data (outliers, unstable signal at the start of the run, loss of signal due to insufficient amount of solution) were removed using the Matlab script of Paris *et al.* (2013). Instrumental mass bias drift was corrected using the bracketing isotope standard analysed before and after each sample analysis (Paris *et al.* 2013, Paris 2023).

Three blanks were prepared to quantify the S contamination during the wet chemistry and purification procedure. They had a mean $\delta^{34}\text{S}_{\text{VCDT}}$ value of $3.23 \pm 0.91\text{‰}$ and contained 2 nmol S. Three independent samples of OSIL Atlantic Seawater were purified following the same purification procedure and run on the MC-ICP-MS to assess the repeatability of the column purification procedure and the instrumental bias of the MC-ICP-MS. These three seawater samples gave a mean $\delta^{34}\text{S}_{\text{VCDT}}$ value of $21.27 \pm 0.16\text{‰}$ (intermediate repeatability given as 95% confidence interval of the population), consistent with MC-ICP-MS values obtained by Das *et al.* (2012; $21.11 \pm 0.40\text{‰}$), Craddock *et al.* (2008; $21.18 \pm 0.27\text{‰}$) and Paris (2023; $21.14 \pm 0.08\text{‰}$), but slightly higher than the values obtained by Paris *et al.* (2013; $20.97 \pm 0.10\text{‰}$).

IRMS

We also measured the S isotopic compositions of the samples on-line using the Thermo Scientific EA IsoLink IRMS System at the CRPG. Test portions of 2–16 mg of each sample were wrapped in a tin capsule, to which approximately 2 mg of vanadium pentoxide was added. The tin capsules were then transferred into an autosampler and combusted by flash pyrolysis ($\sim 1400^\circ\text{C}$) in a combustion reactor consisting of a quartz tube filled with tungsten oxide and pure copper. The gases produced during combustion (N_2 , CO_2 , and SO_2) were separated on a chromatographic column and the sulfur isotopic composition was measured with a Thermo Scientific Delta V Advantage continuous flow IRMS. The sulfur isotopic compositions ($\delta^{34}\text{S}$) of sulfates were determined by comparison with three international reference materials routinely included during analyses: (i) IAEA S1 (silver sulfide, $\delta^{34}\text{S} = -0.3\text{‰}$); (ii) IAEA S2 (silver sulfide, $\delta^{34}\text{S} = +22.62\text{‰}$); and (iii) NBS 123 (sphalerite, $\delta^{34}\text{S} = +17.44\text{‰}$). $\delta^{34}\text{S}$ values are reported in delta notation relative to VCDT and the repeatability on the three international reference materials

was better than 0.3%. In addition, vanadium pentoxide blanks were measured between runs of reference materials and of each sample to ensure that all S was extracted from the metallic samples. Three measurements were performed for each sample and six measurements for each reference material.

The signal from the thermal conductivity detector was calibrated against both international and in-house reference materials used to calculate S mass fractions: (i) BBOT (7.44 g/100 g S); (ii) GSJ JSD-2 (stream sediment, 1.34 g/100 g S); (iii) USGS GXR-4 (copper mill-head, 1.77 g/100 g S); (iv) RIAP DVG (granite, 0.14 g/100 g S); and (v) USGS SDC-1 (mica schist, 0.067 g/100 g S). The differences between the certified and measured values of the reference materials (2s) are expected to be lower than 10% for [S] < 1000 μg g⁻¹ and around 5% for [S] > 1000 μg g⁻¹.

SIMS

For SIMS analyses, samples were pressed into high-purity indium metal mounts, and then mechanically polished using a vibrating polisher in a mixed solution of ethanol and 1 μm diamond powder for 6 h. Finally, samples were gold coated. Samples were left in an oven (at 90 °C) and/or a degassing bench for at least 24 h, then in the instrument airlock for at least another 24 h to ensure the thorough removal of any adsorbed volatiles before introduction into the sample chamber.

Two SIMS sessions were performed to analyse the ³⁴S/³²S_{VCDT} ratios of all samples: session 1 on a SIMS CAMECA IMS 1270 E7 and session 2 on a SIMS CAMECA IMS 1280 HR2, both at the CRPG. In both cases, a primary Cs⁺ beam was used with an acceleration voltage of 10 kV and an intensity of 3 nA, a 15-μm-diameter beam scanned over an area of 20 μm × 20 μm, and a secondary ion extraction potential of 20 kV. To minimise any surface contamination, sample surfaces were pre-sputtered for 90 s over an area of 25 μm × 25 μm prior to signal acquisition. Each analysis consisted of forty cycles of 5.0 s measurements with a mass resolution of 5000 (slit 2). For both sessions, ³²S and ³⁴S were measured on multi-collection mode on two off-axis detectors. ³²S was measured on a Faraday cup (FC) equipped either with a 10¹¹ Ω preamplifier card (session 1) or with a 10¹² Ω preamplifier card (session 2). For session 1, ³⁴S was measured on a 10¹¹ Ω FC for samples containing ≥ 5000 μg g⁻¹ S and with an electron multiplier (EM) for samples with lower S contents, whereas for session 2, ³⁴S was measured on a 10¹² Ω FC for samples containing ≥ 1000 μg g⁻¹ S and with an EM for samples with lower S contents.

Over the course of two sessions, all samples were analysed, but eleven samples (F95S1, F95S50, F95SP4, F90S1, F90S4, F90S50, F90SP4, F80S4, F80S10, FeSiS1, FeSiS4 and FeSiS10) were measured during both sessions for comparison. Sample F90S4 was analysed multiple times during each session to determine the aging of the EM, which is linear with time. The data presented in Table 3 are therefore corrected from FC yields and backgrounds, from EM aging by a careful monitoring of the drift, as well as from the EM deadtime that is determined at the beginning of each session.

Results and discussion

Microstructural and compositional description of the metallic samples

Upon quenching, the melt spinning experiments produced various microstructures (Figure 2) depending on the volatile content, the Fe-Ni (±Si) ratio, and the success of the quenching process; several textures could also occur for the same composition. Here, the samples investigated include what we refer as: (i) ribbons and sparkles, which are about ~20–100 μm thick and represent successful quenches; (ii) feathers, which are flat with one pointed end and the other wider and rounded, and splashes, which are reminiscent of a drop that crashed into the chamber walls (Figure 2b); and (iii) small beads, whose thicknesses vary between 100 μm and 1 mm. Feathers, splashes, and beads are associated with slower quench rates.

Most of the processed compositions show featureless microstructures without Fe, Ni, and Si chemical heterogeneities. This is expected with the melt-spinning process due to the high cooling rates (> 10⁵ K s⁻¹) and compositions that fall into those of amorphous (bulk) alloys, also known as metallic glasses, i.e., 70–85 (Fe, Ni) and 15–30 (Si,S) (Inoue et al. 1978). However, several alloys beyond this compositional range do not form metallic glasses because their compositions are more likely to crystallise (Greer 1993). This is the case for silicon-free samples with low sulfur contents (e.g., F80S1, F80S4, F90S1, F90S4) that present microstructures typical of the solidification of metallic alloys (Figure 3a). Figure 2a-c show backscattered electron images, while Figure 2d-f show chemical maps obtained with EDS in SEM. When nickel and sulfur contents increase, the microstructure becomes more dendritic, and associated micro-segregations are more pronounced. In dendritic microstructures, the heterogeneity scale is that of secondary arms spacings (Dantzig and Rappaz 2016). Still, the secondary arms distance in the samples, and associated micro-segregations

remains at the scale of a few micrometres, so the use of a defocused beam ($\geq 15 \mu\text{m}$ in diameter) was sufficient to average the S contents and obtain a dispersion of the EPMA data generally around 10% (only reaching 30% for F8OSP1 and FeSiSP2).

The S mass fractions measured by EPMA and the CS analyser are in good agreement within measurement repeatability, expressed by the standard deviations on six and three measurements, respectively, for each sample (Table 1). These S mass fractions are very comparable to the S contents expected from the starting materials, implying that no significant S loss occurred during melting. However, we note that for most samples containing $> 1 \text{ g}/100 \text{ g}$ S, the measured S mass fractions were systematically higher in the EPMA data. This overestimation (by 10–30%) may result from the use of pyrite as a reference material for the calibration of S analyses by EPMA; because pyrite contains significantly more S ($> 53 \text{ g}/100 \text{ g}$) than our samples, it may not be the most suitable reference material. Sulfur mass fractions in the four samples analysed by IRMS were lower than those obtained using the CS analyser. Although slightly outside the error bars, the difference between the concentrations determined using these two methods was not very significant, especially considering the textural heterogeneities of samples containing $> 1000 \mu\text{g g}^{-1}$ S. The lower S contents determined by IRMS, compared with those determined using the CS analyser, mainly concern samples F8OS50 and F8OSP1, suggesting that the difference between the concentrations determined using these two methods is not consistent. In addition, because these samples are not homogeneous, we cannot exclude that the 10 mg sampling for IRMS was not as representative as the 50 mg sample measured with the CS analyser. Therefore, we henceforth consider only the CS analyser data when building the SIMS calibration curves in this study.

SIMS calibration curves

The SIMS calibration curves produced herein are presented in Figure 4. We compare the total S mass fractions determined using the CS analyser with the SIMS measurements of $^{32}\text{S}/I_p$, where I_p is the intensity of the SIMS primary beam measured at each analysis. Using such ratio allows to prevent scattering of the ^{32}S counting due to potential variation in primary beam intensity. The representation chosen in Figure 4a allows the visualisation of the S measurements of samples with different S contents and Fe-Ni (\pm Si) ratios, which is necessary to examine the potential matrix effects on the SIMS analyses of S in metal

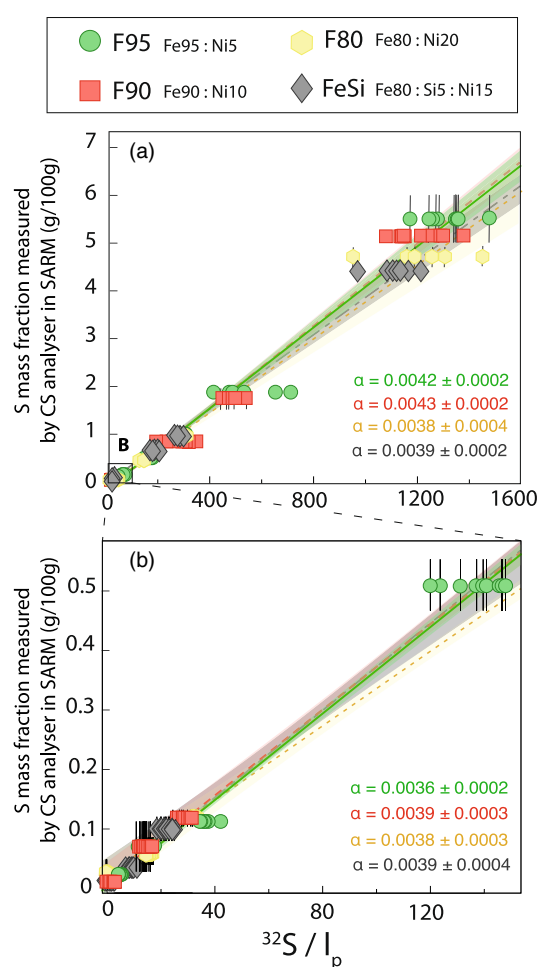


Figure 4. Calibration curves of S mass fraction measurements in two SIMS sessions (session 1 on the SIMS CAMECA IMS 1270 E7 and session 2 on the SIMS CAMECA IMS 1280 HR2), based on the known S contents measured by the CS analyser (SARM, CRPG). (a) All samples; (b) low-S samples (up to $5000 \mu\text{g g}^{-1}$ S for F95 and $1000 \mu\text{g g}^{-1}$ S for F90, F80, and FeSi). The $^{32}\text{S}/I_p$ ratios from both SIMS sessions are undistinguishable for the same samples. The variously dashed lines represent the best-fit linear regression (using the maximum likelihood with over-dispersion) for each Fe-Ni (\pm Si) ratio, and the light-coloured envelopes represent the 2s confidence levels on the best-fit slopes (produced using IsoplotR; Vermeesch 2018).

alloys. The calibration curves show good proportionality between the S mass fractions determined by CS analyser and the SIMS measurements, with a mean slope of 0.0041 ± 0.0004 ($r^2 = 0.9845$ for F95, 0.9843 for F90, 0.9798 for F80, and 0.9897 for FeSi). In Figure 4, the zero-intercept slopes are shown with their 95% confidence level envelopes (2s).

Table 2.
Measurement results for $\delta^{34}\text{S}$ from MC-ICP-MS Neptune Plus analyses of samples undertaken at the CRPG

Sample	$\delta^{34}\text{S}$ 1	1SE	$\delta^{34}\text{S}$ 2	1SE	Averaged $\delta^{34}\text{S}$	Measurement repeatability	Averaged relative intensity
F95S1	14.69	0.07	14.69	0.05	14.69	0.13	0.13
F95S10 #2	16.05	0.02	16.05	0.02	16.05	0.04	0.69
F95S10 #3	15.88	0.02	15.84	0.02	15.86	0.04	0.56
F95SP1	15.94	0.02	15.92	0.02	15.93	0.03	0.71
F95SP2	16.05	0.02	15.90	0.02	15.98	0.04	0.68
F95SP4	16.00	0.02	15.96	0.02	15.98	0.04	0.99
F90S1	13.87	0.06	14.22	0.06	14.05	0.13	0.13
F90SP1	16.07	0.02	16.02	0.02	16.04	0.04	0.63
F90SP4 #1	15.85	0.01	15.81	0.02	15.83	0.03	0.85
F90SP4 #3	15.66	0.02	15.67	0.02	15.66	0.03	0.85
F80SP1	16.06	0.03	16.09	0.03	16.08	0.05	0.63
F80SP4	15.98	0.02	16.03	0.02	16.01	0.04	0.78
FeSi1	12.99	0.07	12.75	0.07	12.87	0.14	0.08
FeSiS50 #1	16.38	0.03	16.32	0.03	16.35	0.05	0.44
FeSiS50 #2	16.09	0.02	16.09	0.02	16.09	0.03	0.65
FeSiS50 #3	16.13	0.02	16.21	0.02	16.17	0.05	0.51
FeSiSP1	16.09	0.02	16.07	0.03	16.08	0.04	0.65
FeSiSP4	15.93	0.01	15.92	0.02	15.92	0.03	0.65
Sw #1	21.21	0.02	21.17	0.02	21.19	0.06	0.49
Sw #2	21.35	0.02	21.35	0.02	21.35	0.06	0.48
Sw #3	21.30	0.05	21.26	0.02	21.28	0.11	0.50
FeS #1	15.97	0.02	15.90	0.02	15.94	0.07	0.76
FeS #2	15.93	0.02	15.89	0.03	15.91	0.07	0.77
FeS #3	15.93	0.03	15.96	0.03	15.95	0.07	0.63
FeS #4	16.01	0.03	16.01	0.03	16.01	0.08	0.53

Uncertainties (1s) on the individual $\delta^{34}\text{S}_{\text{VCDT}}$ (‰) values reflect the measurement precision (here expressed as standard error, 1SE), i.e., as explained in the main text, which relates to the instrumental variability over the fifty cycles. $\delta^{34}\text{S}$ 1 and $\delta^{34}\text{S}$ 2 are two individual MC-ICP-MS measurements of the same solution of a single sample. The uncertainty (1s) of the averaged $\delta^{34}\text{S}_{\text{VCDT}}$ values is the measurement repeatability calculated using the measurement precision (“internal error”) multiplied by the standard deviation of the END. ‘#’ indicates full duplicates of a sample (including independent weighing and column chemistry). The averaged relative intensity is the intensity relative to the bracketing standard (see main text), averaged for the two runs.

The central result of this study is that the calibration curves are indistinguishable from one another, regardless of the chemistry of metal alloys. At high S concentrations, the large dispersion of $^{32}\text{S}/\text{I}_p$ values is explained by the textural and S content heterogeneity of the samples (Figure 4). Interestingly, this does not affect the slopes of the calibration curves within the precision values of the slope calculation for any Fe-Ni ($\pm\text{Si}$) composition, whether considering all samples (Figure 4a) or only the homogeneous samples ($\leq 5000 \mu\text{g g}^{-1}$ S, Figure 4b). This is true for Ni contents varying from 5 to 20 g/100 g and with the addition of ~ 5 g/100 g of Si. Therefore, matrix effect on the S content measurements in Fe-Ni ($\pm\text{Si}$) metal alloys appears to be insensitive to the chemistry of the samples within the range explored here.

Isotopic abundance ratio measurements

Isotopic data presented in Table 2 are both background- and drift-corrected, and are reported as

provisional reference $\delta^{34}\text{S}_{\text{VCDT}}$ values assuming that the $\delta^{34}\text{S}_{\text{VCDT}}$ value of the isotope standard IAEA-S1 is -0.3‰ (Ding *et al.* 2001, Paris *et al.* 2013, Paris 2023). Comparing the signal measured for each sample analysis to that of the bracketing isotope standard solutions measured before and after the sample allows us to calculate the relative signal intensity of each analysis (Table 2) and thus estimate the yield of the entire extraction and purification process. Whereas S dilution prior to MC-ICP-MS analysis was performed to reach 87.5% of the BISS sulfate concentration, the actual relative intensity for the 29 analyses ranged between 12 and 99% (Figure 5). A first possible source of discrepancy is weighing errors given to the nature of the samples, which are sensitive to static effects. Relative intensities above 87.5% likely derive from either insufficient dilution of the sample before analysis, which suggests that the amount of S in the purified sample was underestimated. This is the case at least for sample F95SP4, whose S content was only estimated — and not yet measured using the CS analyser — at the time of analysis.

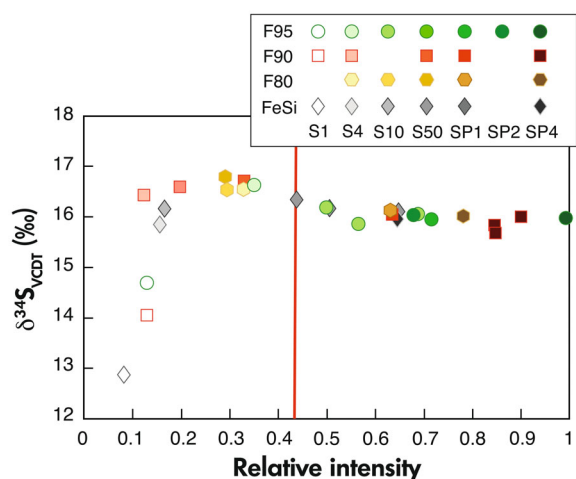


Figure 5. $\delta^{34}\text{S}_{\text{VCDT}}$ values obtained by MC-ICP-MS (ThermoScientific Neptune Plus) as a function of their relative signal intensity, i.e., their signal intensity compared with that of the bracketing standard. The eleven independent samples (seventeen, including replicates) with relative intensities ≥ 0.44 (red line) have stable $\delta^{34}\text{S}_{\text{VCDT}}$ values of $16.01 \pm 0.31\text{‰}$ (2s, standard deviation on the calculated mean over the seventeen measurements).

In contrast, relative intensities significantly lower than 87.5% (i.e. lower than 40 %) do not necessarily derive from an overestimation of the S contents, except for sample F90SP1. For other samples, such low relative intensities may reflect sample loss during the sample manipulation steps. A possibility could be incomplete sulfate recovery

after the iron-oxide precipitation step during the basification of the samples if the precipitation somehow also trapped sulfate, or if H_2S was lost during evaporation of the acid solution.

The blank contribution is negligible for most samples in which at least 30 nmol S was analysed, but this is not the case for low-S samples in which < 10 nmol S was analysed. Indeed, in samples containing 100 and 400 $\mu\text{g g}^{-1}$ S, we can assume that the blank contribution represents 20 and 5%, respectively, of the sample analysed (2.1 ± 0.1 nmol S). Therefore, the $\delta^{34}\text{S}_{\text{VCDT}}$ values of those low-S samples are significantly lower than those of the other samples because they are contaminated by the isotopic composition of the procedural blank ($3.23 \pm 0.91\text{‰}$) (Figure 5).

Among the twenty-nine analyses performed by MC-ICP-MS, seventeen had relative signal intensities that we consider to be acceptable (≥ 0.44 , i.e., $< 50\%$ loss of S); accounting for triplicate analyses of F95S10, F90SP4 and FeSiS50, this corresponds to eleven independent samples. These eleven samples show a stable $\delta^{34}\text{S}_{\text{VCDT}}$ value of $16.01 \pm 0.31\text{‰}$ (Figures 5, 6). The precision is reported at the 95% confidence interval (2s) and represents full procedural repeatability. The mean $\delta^{34}\text{S}_{\text{VCDT}}$ value of the F95S10 triplicates is $16.03 \pm 0.33\text{‰}$, that of the F90SP4 triplicates is $15.84 \pm 0.37\text{‰}$, and that of the FeSiS50 triplicates is $16.20 \pm 0.27\text{‰}$. Although most samples with relative signal intensities ≥ 0.44 have high S contents, the fact that the F95S10 and FeSiS50 triplicates (containing 1000 and 5000 $\mu\text{g g}^{-1}$ S, respectively) have the same

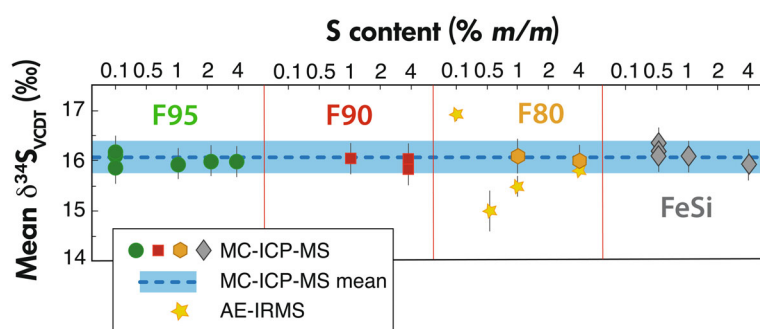


Figure 6. $\delta^{34}\text{S}_{\text{VCDT}}$ results by MC-ICP-MS (ThermoScientific Neptune) obtained for samples with a relative signal intensity ≥ 0.44 for each Fe-Ni ($\pm\text{Si}$) composition (symbols as in Figures 4 and 5) and different S contents (x-axes for each composition). The dashed line shows the mean value of 16.01‰ , and the blue shaded area represents the standard deviations on all MC-ICP-MS measurements ($\pm 0.31\text{‰}$). Bars on the MC-ICP-MS data points represent the intermediate measurement precisions, i.e., the measurement precision (1s) multiplied by the END distribution (1.96). Stars are data from IRMS (Thermoscientific Delta V); despite the variability of IRMS results at low S contents, the $\delta^{34}\text{S}_{\text{VCDT}}$ value of F80SP4 is in relative agreement with the MC-ICP-MS results. Note the consistency of the MC-ICP-MS $\delta^{34}\text{S}_{\text{VCDT}}$ values of all the samples, regardless of Fe-Ni ($\pm\text{Si}$) composition or S content.

$\delta^{34}\text{S}_{\text{VCDT}}$ values (within intermediate measurement precision) as higher-S samples suggests that those samples' S contents did not affect their $\delta^{34}\text{S}_{\text{VCDT}}$ values. We estimated intermediate measurement precisions as follows. Each purified sample was run only twice; therefore, we cannot calculate a standard deviation. Instead, the entirety of a given run is used to calculate the mean and standard deviation of "error normalised deviates" (ENDs; John and Adkins 2010) as:

$$\text{END} = \frac{R_1 - R_2}{\sqrt{\sigma_1^2 - \sigma_2^2}} \quad (1)$$

where R_1 and R_2 are the measured isotopic ratios for two runs and σ_1 and σ_2 are the measurement precision associated with these ratios. The calculation of the error-normalized deviates yields an END distribution with a standard deviation of 1.96. This value was applied as a multiplying factor to the root mean square of the two individual standard errors on the measurements used to calculate the averaged $\delta^{34}\text{S}$ to evaluate measurement repeatability (Paris *et al.* 2013). Measurement precision is estimated using the standard error, i.e., the deviation of each point from the mean divided by the square root of the number of cycles ($n = 50$). Measurement precision is explained to the first order by processes such as counting statistics and Johnson noise (John and Adkins 2010 or Paris *et al.* 2013). The value of 1.96 means that intermediate reproducibility is about twice as large as the measurement precision.

Based on these results, the overall reproducibility of the eleven samples is indistinguishable from the repeatability of triplicate analyses, suggesting that each sample is homogeneous at the "bulk" scale during MC-ICP-MS analyses, and that all reference materials are isotopically identical within analytical error. In addition to the absence of any significant S loss between the initial S contents of the materials and starting those of the produced alloys, this indicates that there was no significant S isotopic fractionation during the melt spinning experiments. Besides, the stable $\delta^{34}\text{S}_{\text{VCDT}}$ value of $16.01 \pm 0.31\text{‰}$ is identical within error to that determined in the starting FeS, our source of S, $15.95 \pm 0.08 \text{‰}$ (Table 2). This value for the FeS corresponds to a mean of four independent measurements of the mass of the same sample, each of which was analysed twice by MC-ICP-MS, with relative intensities always ≥ 0.53 .

Results from IRMS analyses are compared with MC-ICP-MS data in Figure 6. The results for F8OSP4 are in agreement with the MC-ICP-MS results within measurement precision. In contrast, those for F8OS10, F8OS50 and F8OSP1 differ beyond

the analytical repeatabilities of the two methods. Nonetheless, these differences are within 1.5‰ of the mean $\delta^{34}\text{S}_{\text{VCDT}}$ value determined by MC-ICP-MS ($16.01 \pm 0.31\text{‰}$). Therefore, these two analytical methods, with very different S extraction procedures from the metal alloys, delivered comparable results. This agreement confirms the validity of the S chemical extraction procedure developed herein.

Investigation of matrix effects on instrumental mass fractionation during SIMS analyses

In this subsection, we consider the constant $\delta^{34}\text{S}_{\text{VCDT}}$ value of $16.01 \pm 0.31\text{‰}$ obtained by MC-ICP-MS to be the "true" $\delta^{34}\text{S}_{\text{VCDT}}$ value of the samples. We used this value to determine the instrumental mass fractionation (IMF, in ‰) during SIMS S analyses in the Fe-Ni (\pm Si) metal alloys, calculated as:

$$\text{IMF} = \delta^{34}\text{S}_{\text{SIMS}} - \delta^{34}\text{S}_{\text{true}} \quad (2)$$

Multiple IMF values were obtained because measurements were performed during two different SIMS sessions (session 1, SIMS CAMECA IMS 1270 E7; session 2, SIMS CAMECA IMS 1280 HR2), and for each session, different pairs of detectors were used to measure S-poor and S-rich samples (see Methods). To directly compare the effect of the chemical composition of metal alloys on the IMF, we overcame the yield effects of the different detectors by fixing the IMF of a sample as an anchor, and correcting the IMFs of all the other samples relative to that anchored value. Figure 7 shows no effect of metal alloy chemical composition or S content on the corrected IMF values. Most samples show no significant deviation from the averaged corrected IMF, except for sample F9OS1. This may be because analyses of sample F9OS4 have not been bracketed with sample F9OS1, used to monitor the EM aging through the sessions. Therefore, we assume that the EM aging for this sample may not have been totally corrected. Differences in IMF within a single sample between session 1 and session 2 (Figure 7) likely indicate their heterogeneities, as for instance sample F8OS10.

Consequently, as for the S content calibration curves, we conclude that there was no significant matrix effect on the IMF during S isotopic measurements by SIMS, neither due to the alloys' Fe-Ni (\pm Si) contents nor their S contents.

Twelve samples were measured on FC-EM during both SIMS sessions, we averaged their IMFs by FC-EM during session 1 ($\overline{\text{IMF}}_{\text{FC-EM},1}$) and, separately, those measured during session 2 ($\overline{\text{IMF}}_{\text{FC-EM},2}$), and the difference between the means was calculated as $\overline{\Delta}_{\text{FC-EM},2-1} = \overline{\text{IMF}}_{\text{FC-EM},2} - \overline{\text{IMF}}_{\text{FC-EM},1}$. To directly compare the FC-EM

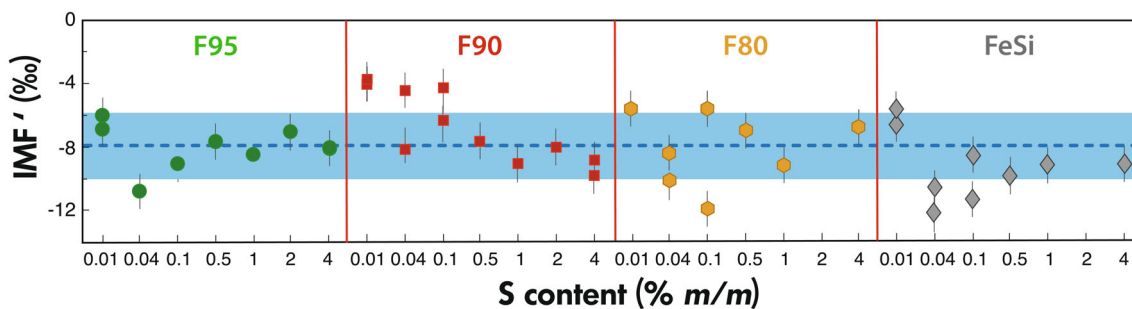


Figure 7. Instrumental mass fractionation, corrected relative to several anchors (IMF' , ‰) as a function of metal alloy composition (for each F95, F90, F80, and FeSi series) and S content. The IMF obtained during session 1 for sample F95S10, analysed by FC-FC was chosen as an anchor to correct the IMF of all the samples measured in session 2 (2,i) measured by FC-FC because this sample was measured during both sessions. Such as:

$$\Delta_{FC-FC} \text{ bold} = IMF_{F95S10,2} - IMF_{F95S10,1} \text{ and } IMF'_{FC-FC,2,i} \text{ bold} = IMF_{FC-FC,2,i} - \Delta_{FC-FC}$$

values from the two sessions, the values of all the samples measured by FC-EM during session 2 were then corrected for this difference as $IMF'_{FC-EM,2,i} = IMF_{FC-EM,2,i} - \bar{\Delta}_{FC-EM,2-1}$. Similarly, the FC-EM values from session 1 and the corrected FC-EM values from session 2 were adjusted to the anchor FC-FC value for session 1, as:

$$IMF'_{FC-EM,1,i} = IMF_{FC-EM,1,i} - \bar{\Delta}_{FC-EM,1} \quad (3)$$

where $\bar{\Delta}_{FC-EM,1} = \overline{IMF}_{FC-EM,1} - IMF_{F95S10,1}$

and for session 2 as:

$$IMF'_{FC-EM,2,i} = IMF_{FC-EM,2,i} - \bar{\Delta}_{FC-EM,1} \quad (4)$$

Recommended samples for S analyses and uncertainties on unknown analyses

Although the low solubility of S in Fe-Ni (\pm Si) metal alloys caused heterogeneities in some of our samples, we selected eight of our twenty-eight synthesised samples as suitable for use as reference materials: F95S1, F95S4, F95S10, F95S50, F90S1, F80S1, FeSiS4, and FeSiS10 (marked in dark grey in Table 3). We selected these samples based on two criteria: (i) standard deviation < 10% (1s) for $^{32}S/lp$ in each sample (15 of 28 samples meet this criterion), and (ii) standard deviation < 10‰ (1s) for $\delta^{34}S_{SIMS}$ (8 of the 15 samples satisfying criterion (i) also meet this criterion). Using only these eight reference materials, we obtained a slope of 0.0039 ± 0.0002 ($r^2 = 0.984$) for the calibration curve, identical to those of the calibration curves for each sample composition within the precision of the slope calculation (Figure 4). It is possible to use samples of varied Fe-Ni (\pm Si) compositions

as reference materials because no matrix effect was detected on the calibration curves or the IMF. Since these samples contain < 5000 $\mu\text{g g}^{-1}$ S, we recommend they be used as S-undersaturated metal alloys. That said, because the slope of this calibration curve is identical to those obtained using samples containing up to 4 g/100 g S, and because we did not observe any S content effect on the IMF, these new reference materials could be used for unknown samples richer in S if necessary, as long as a largely de-focused beam ($\geq 30 \mu\text{m}$ in diameter) is used to average out textural and/or S-content heterogeneities. This method may be useful to determine S contents, but will induce large errors on the determined $^{34}S/^{32}S_{VCDT}$ ratios.

Finally, for sulfides and sulfide-bearing metal blobs in experimental samples, we still recommend bulk analytical methods, either for analysis as a gas phase (e.g., IRMS, as described here or following Labidi *et al.* 2016) or in solution following the method developed herein (see Methods). Indeed, the S extraction method developed in this study, coupled with MC-ICP-MS analysis, reduces the errors on determining $\delta^{34}S_{VCDT}$ to on the order of $\pm 0.3\%$.

Conclusions

To address the lack of S-bearing metallic reference materials for SIMS analyses, we produced a series of eight suitable Fe-Ni (\pm Si) alloys using the 'melt spinning' method to quench them at $\sim 10^4$ – 10^6 K s^{-1} . Despite the rapid quench rates, these materials are crystallised, though this does not seem to have any influence on their S contents and isotopic compositions: crystallisation occurred during the quench and produced variably oriented but compositionally homogenous Fe-Ni (\pm Si) crystals. We also note that the initial S content and isotopic composition of these

Table 3. Measurement results from two SIMS sessions, $^{32}\text{S}/\text{Ip}$ and the IMF' calculated as explained in Figure 7

Samples	Session 1				Session 2			
	Detectors	n	$^{32}\text{S}/\text{Ip}$	IMF' (‰)	Detectors	n	$^{32}\text{S}/\text{Ip}$	IMF' (‰)
F95S1	FC-EM	6	5 ± 1	-6.00 ± 1.11	FC-EM	3	5 ± 1	-6.81 ± 1.11
F95S4					FC-EM	6	15 ± 2	-10.81 ± 1.11
F95S10					FC-FC	6	36 ± 3	-9.11 ± 1.11
F95S50	FC-FC	6	143 ± 4.46	-7.66 ± 0.73	FC-FC	6	125 ± 6	-7.70 ± 0.93
F95SP1	FC-FC	6	287 ± 9	-8.48 ± 1.13				
F95SP2	FC-FC	6	533 ± 117	-7.07 ± 1.15				
F95SP4	FC-FC	6	1355 ± 68	-8.08 ± 1.12	FC-FC	6	1219 ± 43	-7.88 ± 1.12
F90S1	FC-EM	6	4 ± 1	-3.75 ± 1.11	FC-EM	3	4 ± 1	-4.00 ± 1.11
F90S4	FC-EM	6	14 ± 1	-4.39 ± 1.11	FC-EM	12	15 ± 1	-8.24 ± 1.11
F90S10	FC-EM	9	28 ± 2	-4.21 ± 1.16	FC-FC	6	28 ± 8	-6.26 ± 1.16
F90S50	FC-FC	6	138 ± 8	-7.61 ± 1.16				
F90SP1					FC-FC	24	264 ± 33	-9.06 ± 1.17
F90SP2	FC-FC	6	473 ± 26	8.01 ± 1.16				
F90SP4	FC-FC	8	1333 ± 93	-8.81 ± 1.14	FC-FC	6	1125 ± 28	-9.81 ± 1.14
F80S1					FC-EM	6	2 ± 1	-5.57 ± 1.11
F80S4	FC-EM	6	17 ± 1	-10.19 ± 1.11	FC-EM	3	16 ± 1	-8.36 ± 1.11
F80S10	FC-EM	6	32 ± 5	-11.91 ± 1.14	FC-FC	6	29 ± 2	-5.57 ± 1.14
F80S50	FC-FC	6	133 ± 13	-6.97 ± 1.12				
F80SP1	FC-FC	6	294 ± 8	-9.15 ± 1.12				
F80SP2								
F80SP4	FC-FC	6	1225 ± 168	-6.76 ± 1.12				
FeSIS4	FC-EM	6	3 ± 1	-6.54 ± 1.13	FC-EM	9	3 ± 1	-5.59 ± 1.13
FeSIS10	FC-EM	6	12 ± 1	-10.67 ± 1.11	FC-EM	21	10 ± 1	-12.29 ± 1.11
FeSIS50					FC-FC	6	24 ± 2	-8.48 ± 1.13
FeSISP1					FC-FC	6	195 ± 13	-9.81 ± 1.16
FeSISP2					FC-FC	6	309 ± 34	-9.10 ± 1.14
FeSISP4	FC-FC	6	1116 ± 84	-9.06 ± 1.14				

Uncertainties reflect 2s standard deviations on *n* analyses per sample. Samples highlighted in dark grey are recommended as reference materials for S measurements by SIMS. Those highlighted in light grey can be considered as 'acceptable' if a large number of reference materials is needed for calibration.

materials were not fractionated by S loss. Therefore, these new metallic reference materials are suitable for analyses of metal-bearing high-pressure samples, as well as iron meteorites or metallic phases in meteorites. Several milligrams of these new metallic reference materials are available for distribution, upon request, to various SIMS laboratories worldwide.

We also established a new method of S chemical extraction from a metallic matrix, and thus were able to measure the absolute S isotopic composition of our metallic alloys by MC-ICP-MS. The constant $\delta^{34}\text{S}_{\text{VCDT}}$ values obtained among the analysed samples supports the reliability of the $\delta^{34}\text{S}_{\text{VCDT}}$ value of 16.01 ± 0.31 ‰ for our reference materials.

Acknowledgements

We are grateful to Delphine Lequin for her help during the melt spinning experiments and to Gwladys

Lengaigne for fixing the melt spinning apparatus after an unfortunate incident and for access to the IJL experimental platform. We are thankful to Perrine Mathieu and Pierre-Yves Martin for the Carbon-Sulfur analyses on the SARM platform, and to Nordine Bouden for help with the SIMS. We also thank Catherine Zimmermann and Aimeryc Schumacher who helped Lenny Riquet in the laboratory. All analytical platforms are part of the RéGEF network. This project was funded by ANR JCJC CSI Planet (ANR-22-CE49-0003). This is CRPG contribution 2860.

Scientific editing by Jacinta Enzweiler.



Data availability statement

The data that supports the findings of this study are available in the supplementary material of this article.

References

Craddock P.R., Rouxel O.J., Ball L.A. and Bach W. (2008)
Sulfur isotope measurement of sulfate and sulfide by high-resolution MC-ICP-MS. *Chemical Geology*, 253, 102–113.

Dalou C., Hirschmann M.M., von der Handt A., Mosenfelder J. and Armstrong L.S. (2017)
Nitrogen and carbon fractionation during core–mantle differentiation at shallow depth. *Earth and Planetary Science Letters*, 458, 141–151.

Dantzig J.A. and Rappaz M. (2016)
Solidification: Revised & Expanded. EPFL Press.

Das A., Chung C.H. and You C.F. (2012)
Disproportionately high rates of sulfide oxidation from mountainous river basins of Taiwan orogeny: Sulfur isotope evidence. *Geophysical Research Letters*, 39.

Ding T., Valkiers S., Kipphardt H., De Bievre P., Taylor P.D P., Gonfiantini R. and Krouse R. (2001)
Calibrated sulfur isotope abundance ratios of three IAEA sulfur isotope reference materials and V-CDT with a reassessment of the atomic weight of sulfur. *Geochimica et Cosmochimica Acta*, 65, 2433–2437.

Freyer D. and Voigt W. (2003)
Crystallization and phase stability of CaSO₄ and CaSO₄-based salts. *Monatshefte für Chemie/Chemical Monthly*, 134, 693–719.

Greer A.L. (1993)
Confusion by design. *Nature*, 366, 303–304.

Inoue A., Masumoto T., Kikuchi M. and Minemura T. (1978)
Compositional effect on crystallization of (Fe, Ni, Co)-Si-B amorphous alloys. *Journal of the Japan Institute of Metals*, 42, 294–303.

Labidi J., Cartigny P., Birck J.L., Assayag N. and Bourrand J.J. (2012)
Determination of multiple sulfur isotopes in glasses: A reappraisal of the MORB $\delta^{34}\text{S}$. *Chemical Geology*, 334, 189–198.

Labidi J., Cartigny P. and Moreira M. (2013).
Non-chondritic sulphur isotope composition of the terrestrial mantle. *Nature*, 501, 208–211.

Labidi J. and Cartigny P. (2016)
Negligible sulfur isotope fractionation during partial melting: Evidence from Garrett transform fault basalts, implications for the late-veneer and the Hadean matte. *Earth and Planetary Science Letters*, 451, 196–207.

Labidi J., Shahar A., Le Losq C., Hillgren V.J., Mysen B.O. and Farquhar J. (2016)
Experimentally determined sulfur isotope fractionation between metal and silicate and implications for planetary differentiation. *Geochimica et Cosmochimica Acta*, 175, 181–194.

Li Y., Dasgupta R., Tsuno K., Monteleone B. and Shimizu N. (2016)
Carbon and sulfur budget of the silicate Earth explained by accretion of differentiated planetary embryos. *Nature Geoscience*, 9, 781–785.

Paris G., Sessions A.L., Subhas A.V. and Adkins J.F. (2013)
MC-ICP-MS measurement of $\delta^{34}\text{S}$ and $\Delta^{33}\text{S}$ in small amounts of dissolved sulfate. *Chemical Geology*, 345, 50–61.

Paris G. (2023)
Determination of unbiased $\delta^{34}\text{S}$ and $\Delta^{33}\text{S}$ values by MC-ICP-MS using down to 30 nmol of sulfur. *Geostandards and Geoanalytical Research*, 48, 29–42.

Tkatch V.I., Limanovskii A.I., Denisenko S.N. and Rassolov S.G. (2002)
The effect of the melt-spinning processing parameters on the rate of cooling. *Materials Science and Engineering: A*, 323, 91–96.

Tsuno K., Grewal D.S. and Dasgupta R. (2018)
Core-mantle fractionation of carbon in Earth and Mars: The effects of sulfur. *Geochimica et Cosmochimica Acta*, 238, 477–495.

Speelmanns I.M., Schmidt M.W. and Liebske C. (2019)
The almost lithophile character of nitrogen during core formation. *Earth and Planetary Science Letters*, 510, 186–197.

Vermeesch P. (2018)
IsoplotR: A free and open toolbox for geochronology. *Geoscience Frontiers*, 9, 1479–1493.

Wang W., Li C.H., Brodholt J.P., Huang S., Walter M.J., Li M., Wu Z., Huang F. and Wang S.J. (2021)
Sulfur isotopic signature of Earth established by planetesimal volatile evaporation. *Nature Geoscience*, 14, 806–811.

Supporting information

The following supporting information may be found in the online version of this article:

Table S1. Results from two SIMS measurement sessions, uncorrected averaged $\delta^{34}\text{S}_{\text{VCDT}}$ (‰) and the IMF without any corrections.

This material is available from: <http://onlinelibrary.wiley.com/doi/10.1111/ggr.12584/abstract> (This link will take you to the article abstract).